Supporting Information

Time-Lapse Nanoscopy of Friction in the Non-Amontons and Non-Coulomb Regime

Tadashi Ishida,[†,‡] Takaaki Sato[†], Takahiro Ishikawa,[§] Masatsugu Oguma,[§] Noriaki Itamura,[§] Keisuke Goda,[∥,⊥] Naruo Sasaki[§] & Hiroyuki Fujita[†]*

[†] Institute of Industrial Science, University of Tokyo, Tokyo 153-8505, Japan

[‡] Interdisciplinary Graduate School of Science and Engineering, Tokyo Institute of Technology, Yokohama, Kanagawa 226-8502, Japan

[§] Department of Applied Science, Seikei University, Tokyo 180-8633, Japan

[∥] Department of Chemistry, University of Tokyo, Tokyo 113-0033, Japan

[⊥] Department of Electrical Engineering, University of California, Los Angeles, California 90095, USA

Present Addresses

N.S.: Graduate School of Informatics and Engineering, The University of Electro-Communications, Chofu, Tokyo, 182-8585, Japan

*To whom correspondence should be addressed.

E-mail: ishida.t.ai@m.titech.ac.jp (T.I.)

Silicon anvils with electrostatic microactuators. The silicon anvils with the electrostatic microactuators were produced from a silicon-on-insulator (SOI) wafer using bulk-micromachining and focused ion beam (FIB) etching. Aluminum masks for deep reactive

ion etching (DRIE) were patterned on both sides of the SOI wafer. DRIE and buffered hydrofluoric acid etching were performed on the backside of the SOI wafer whereas DRIE was performed on the front side of the SOI wafer. A silicon bridge structure was cut with FIB etching, resulting in a pair of silicon tips. More details of the fabrication procedure can be found in Ref. (S1). To control the position of the electrostatic microactuators, we used a semiconductor parameter analyzer to precisely adjust the voltage on the actuators with high precision of ±0.018% and hence to control their speed (as we applied to the actuators 100 V at maximum with precision of ±18 mV). This precision in voltage control translates into precision of 0.05 nm in displacement of the anvil. The lowest voltage change speed for controlling the anvils is 2 mV/s, resulting in 0.005 nm/s of the lowest sliding speed.

Force measurement. Our method for measuring the indentation force is analogous to that used in atomic force microscopy. Using TEM's high-resolution images, we measured the positions of the anvils with and without their contact when applying the same electrostatic force on the microactuators and then determined the indentation force by multiplying the difference between the two positions with the spring constant of the electrostatic actuators (75 N/m in our design), which was determined by treating the actuator as a beam member with both ends fixed. Based on the TEM's limited point-to-point resolution in imaging of the edge of the anvils (0.13 nm), we found the FWHM (full width at half maximum) resolution of our force measurement to be 75 N/m × 0.13 nm = 9.8 nN.

Consideration of potential noise on the position of the anvils. The fluctuation of the anvils caused by the thermal energy inside the TEM specimen chamber is determined from T = 300 K

and k = 75 N/m to be 7.4 pm, which is negligible compared with the actuator-driven displacement. The Brownian motion of the anvils is negligible since the environment for the anvils is ultrahigh vacuum and the effect of residual molecules on the anvils is extremely small. On the surface of the tip, stress-assisted diffusion of atoms is dominant.

Imaging apparatus. The time-lapse imaging experiment was conducted inside an ultra-high vacuum TEM with a field emission gun (HF2000-UHV, Hitachi). A specially customized TEM sample holder with nine electrical feedthroughs was used for the electrostatic microactuators. The TEM was operated at 200 kV with a lattice resolution of about 0.2 nm. The video was recorded by a high-sensitivity avalanche image pickup tube (Hitachi UTK-2000) at 30 fps. The current density of the electron beam was 6.2×10^{-8} A/cm^2, which had no appreciable effect on the plastic deformation of the anvils (see Supporting Information Figure S7).

Digital image processing. Total variation denoising[S2,S3] was applied to the captured data to generate the images and movie in Figure 2, and Supporting Information Movie S1. The total variation is defined as the integral of the absolute gradient of an input signal. In the denoising process, the 3D (transverse and temporal) total variation was minimized. Each denoised frame was calculated with twenty-one consecutive original frames in which the target frame is the middle one.

Simulation model of the silicon anvils. A pair of hemispheres was used as a model to simulate the compression and rub of the silicon anvils shown in Figure 2. Both hemispheres are shaped with a diameter and orientation of 7.74 nm and (100), respectively. The Stillinger-Weber

potential was used as a covalent bond of silicon atoms. The base (single atomic layer) of each hemisphere was fixed while atoms in the other part were stabilized with a Monte Carlo (MC) method. The atoms in each stabilized hemisphere were given velocities at 300 K under the Maxwell velocity distribution. The hemispheres were brought into contact with an indentation of 1.66 nm at an approach speed of 2.72 x 10^2 m/s using the MD method. The junction was stabilized again using the MC method. A slight initial displacement was introduced to the lower hemisphere to simulate the experiment. The lateral displacement was performed at a displacement speed of 2.72 x 10^2 m/s and 300 K (using a pair of heat baths attached to the anvil supports) until the breakage of the connection between the hemispheres (specifically, until the formation of the single atomic chain that connects the hemispheres). The time step is 7.72 fs whereas the total time is 76.6 ps.

Phase transformation energetics at the anvil interface. Before the anvils contact, the average energy of each silicon atom in the anvils is -4.14 eV. As the indentation increases, the energy gradually increases up to -3.64 eV at 1.66 nm (indentation stroke), which is beyond the energy limit of being crystalline (-4.1 eV). Hence, the crystalline structure becomes unstable and transforms into a random (amorphous) arrangement. The excessive energy over the limit is dissipated. These energy values in our simulation model agree well with those used in a previous report using the Stillinger-Weber potential.[S4]

Physical significance of the displacement, junction diameter, and tilt angle. The displacement, junction diameter, and tilt angle are defined as shown in Figure 3a because these parameters indicate mechanical input, junction growth, and thinning (volume change in the

junction). While a stress-strain curve is typically used in analysis of results from shear tests, we have found these parameters to be more physically meaningful as the time-resolved morphological information (shape and structure) of the anvils is available for detailed analysis. It is important to note that in our definition of the tilt angle, it is not merely $\tan^{-1}$ (lateral displacement / separation of anvils) which actually holds if the displacement is small, but includes the effect of stress-assisted surface diffusion which decreases the separation between the anvil supports (bases) as the displacement is large. In this sense, the tilt angle is also an indicator of shear strain plus stress-assisted surface diffusion.

Stress-assisted surface diffusion of atoms. Using Eq. 30,[29] the diffusion coefficient in the high-pressure regime can be found to be $D_\sigma = 0.17\ \mathrm{nm^2/s}$ from $s_0 = 0.1\ \mathrm{nm^2/s}$, $\Delta E = 1\ \mathrm{eV}$, $k_B T = 0.0255\ \mathrm{eV}$, $\sigma = 1.54\ \mathrm{GPa}$, and $\Omega = 0.04\ \mathrm{nm^3}$. Assuming that the pressure applied to the anvil junction is constant at 1.54 GPa, by using this diffusion Coefficient value and Eq. 32,[29] the junction volume increased by stress-assisted surface diffusion of atoms is found to be 225 $\mathrm{nm^3}$ while the initial volume is 141 $\mathrm{nm^3}$. Therefore, the increased volume in the junction is given by 60%.

Effect of the time-scale difference between the simulation and experiment. The sliding speed of the lower anvil should have an impact on the dynamics of the anvils' plastic deformation as it changes the relation between their energy dissipation and the energy input into the anvil junction. In order to validate our comparison between the simulation (which is fast on the order of picoseconds due to the nature of computer-based molecular simulations) and the experiment (slow), we used a technique that approximates the actual motion of the anvils in our experiment.

Specifically, in the experiment, since the sliding speed is ultralow (~0.01 nm/s), the anvil junction has enough time to dissipate all the input energy. This situation can be approximated by the MD simulation with the use of heat baths attached to the anvil supports which dissipate the input energy more quickly than the sliding speed which may be orders of magnitude higher than the actual sliding speed in the experiment. In order to further validate the comparison between the simulation and experiment, we compared the MD simulation against the CG method that deals with minimum energy states of atoms which are stabilized after a long period of time (hence, a quasi-static method). As indicated in Supporting Information Figure S8, it is found from the comparison of the MD and CG simulation results that the time-scale difference (or the difference in sliding speed) has no significant influence on the simulation results.

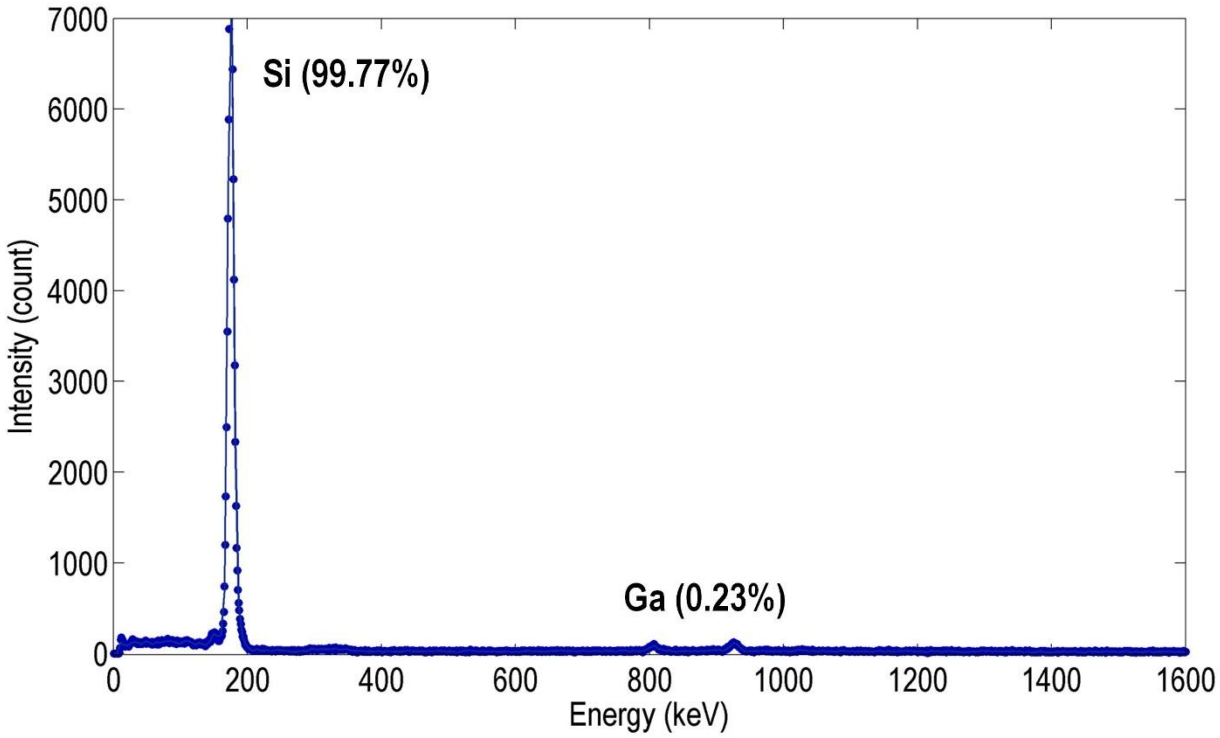

Figure S1. Composition of the anvils. In order to minimize the amount of other materials in the silicon anvils such as gallium (implanted in the process of the FIB milling) and native oxide

(produced in the process of installing the silicon anvils in the TEM imaging system), we used the method of exposing anvil-shaped crystalline silicon surfaces by mechanically hitting cone-shaped silicon tips against each other in the TEM's ultrahigh vacuum chamber multiple times after the FIB milling.[S1] In other words, we used the exposed crystalline regions of the silicon cones as the silicon anvils in our time-lapse nanoscopy experiment. Likewise, using the same method, we eliminated the implanted gallium in the silicon anvils down to 0.23% of the composition. We also removed the oxide layer of the silicon cones (caused by exposure to air) by using the same methods.

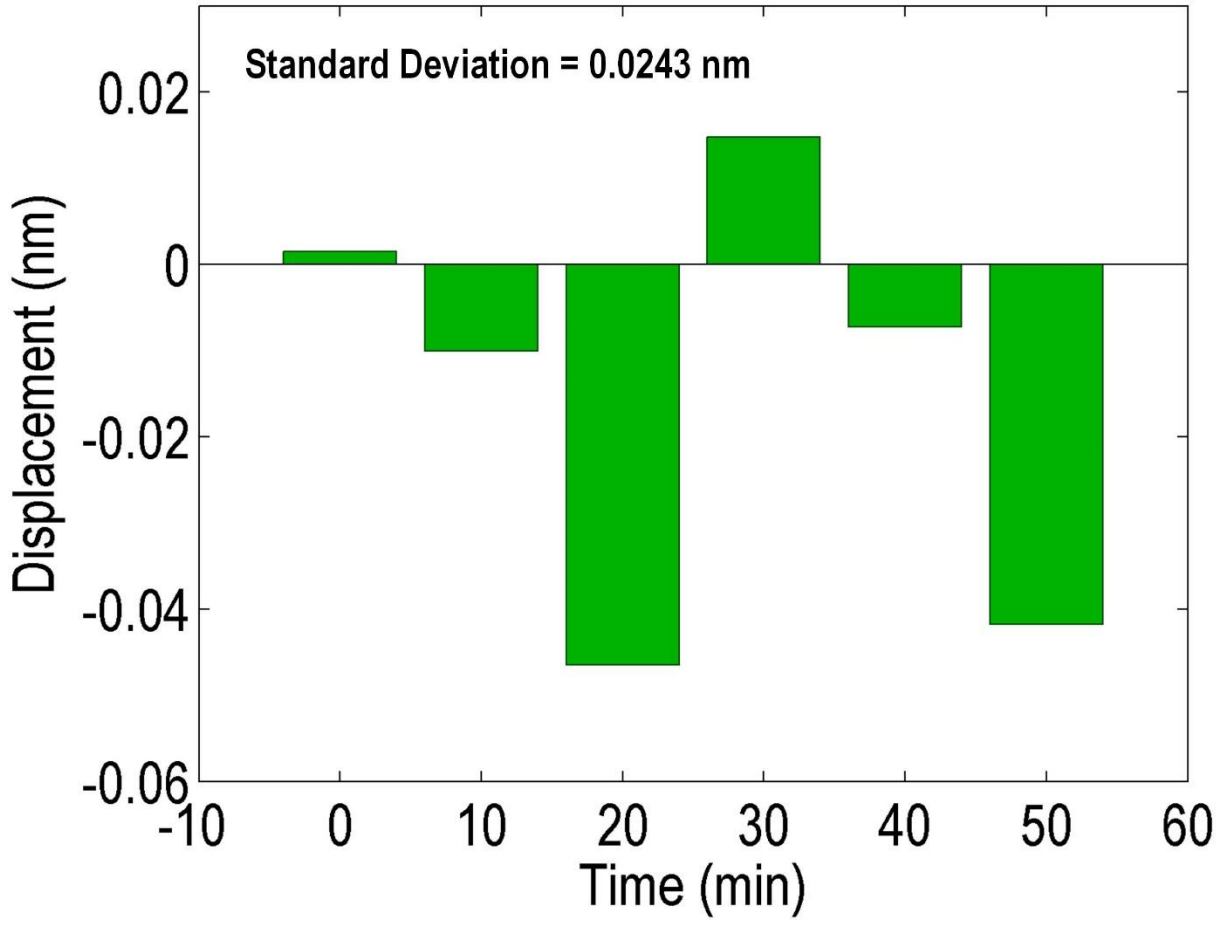

Figure S2. Fluctuations in the position of the lower anvil. The position of the anvil was

measured for duration of 50 min. The standard deviation of the fluctuations is found to be 0.0243 nm, which is much smaller than the total displacement of 16 nm produced by our electrostatic actuator for the lower anvil, and can, hence, be considered to be negligible in our time-lapse nanoscopy experiment.

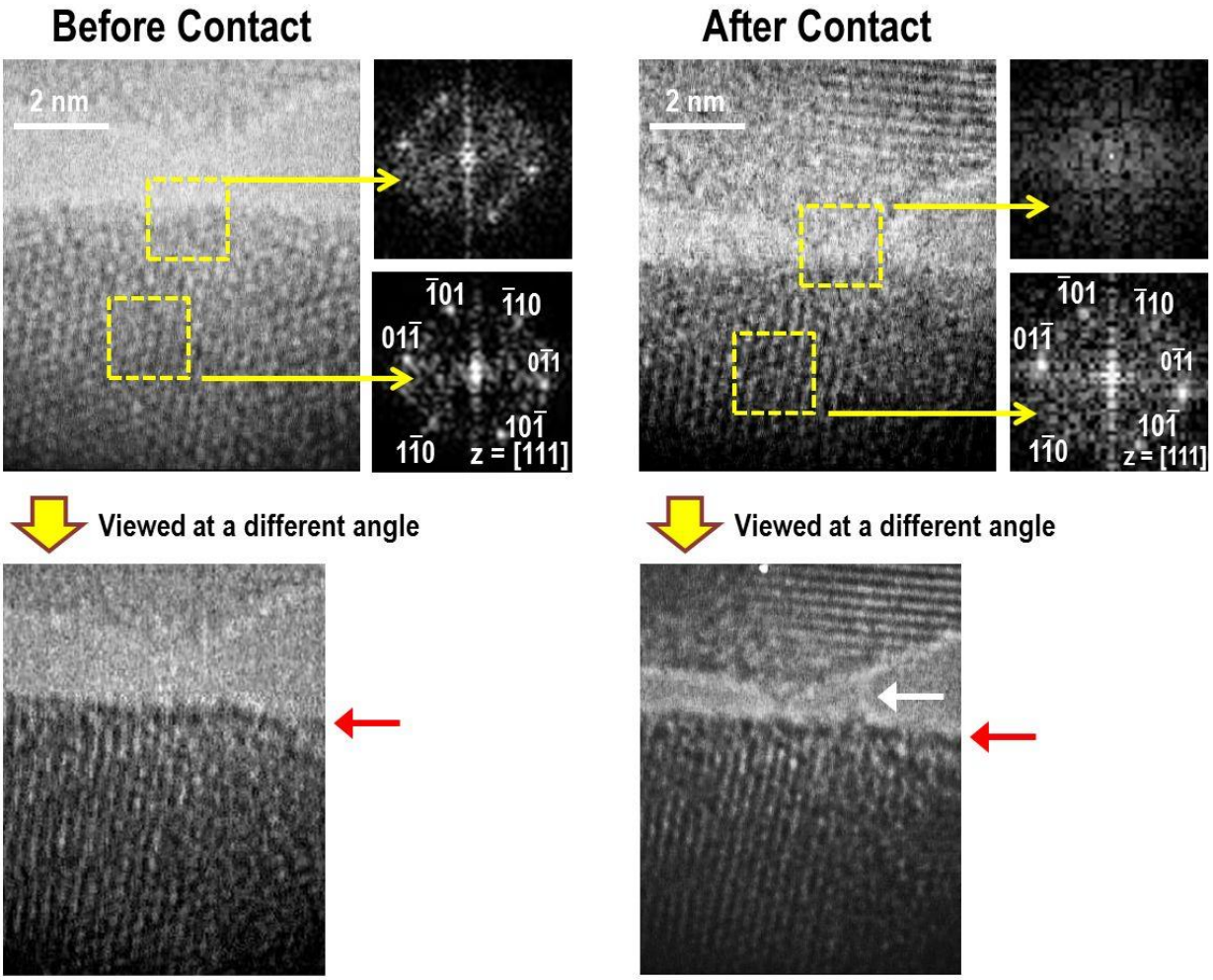

Figure S3. Structural properties of the silicon anvils before and after the contact. Fast Fourier transformation (FFT) images of the dotted regions in the anvil indicate its crystalline structure before the contact. These spots originate from the $\{10\bar{1}\}$ lattice fringe in the TEM image. FFT images of the dotted regions in the anvil indicate that the region distant from the junction

between the anvils is intact and remains crystalline after the contact whereas the structure of the junction becomes amorphous. TEM images of the anvils at a different viewing angle show clear lattice fringes to the very edge of the anvils (indicated by the red arrows) and amorphous structure (indicated by the white arrow) although it is difficult to see more than one lattice fringe at this viewing angle (while more than two lattice fringes can be seen at the viewing angle in the upper panels).

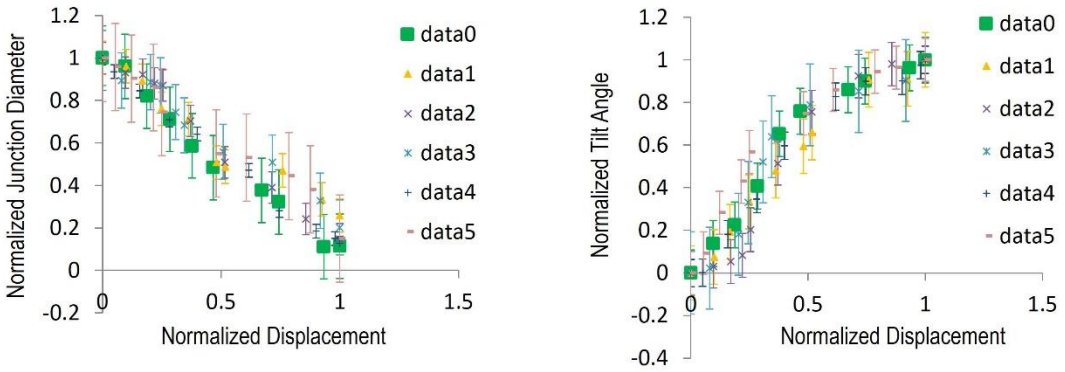

Figure S4. Analysis of experimental data from different measurements. Comparison of experimental data from several measurements. Here, data0 indicates the data shown in Figure 2 and Figure 3b while data1 through data5 are from the additional tests (see Supporting Information Table S1). The error bars come from blur in the acquired TEM images. The figure shows good consistency between the different measurements. Here the normalized displacement, normalized junction diameter, and normalized tilt angle are defined to be the displacement divided by the maximum displacement at the time of the junction breakage, the junction diameter divided by the initial junction diameter, and the tilt angle minus the initial tilt angle divided by the maximum tilt angle minus the initial tilt angle, respectively.

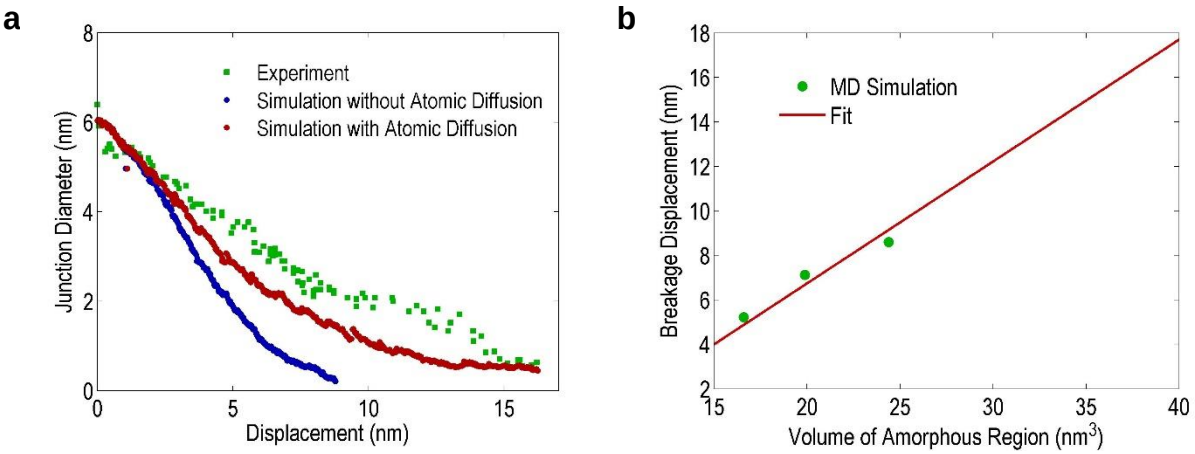

Figure S5. Influence of stress-assisted surface diffusion of atoms on the junction diameter of the anvil junction. (a) Junction diameter with and without stress-assisted surface diffusion of atoms. The continuous increase in the volume of the amorphous region accounts for the decreased rate of change in the junction diameter. (b) Breakage displacement as a function of the volume of the amorphous region. In order to estimate the effect of stress-assisted surface diffusion on the junction diameter, we performed MD simulations with three different initial volumes for the amorphous region (16.6 nm^3, 19.9 nm^3, and 24.4 nm^3) which lead to three different breakage displacements, from which we determined the relation between the volume of the amorphous region and the breakage displacement by fitting the MD simulation data with a linear function. From the relation, we then estimated the junction diameter as a function of displacement for other initial volumes. Finally, assuming that the final volume increase is 80% (77% in the actual observation), we segmented the total displacement by a factor of 17 for a constant increase rate of 5% and then patched the different sections of the functions together to obtain the function shown in (a)**.**

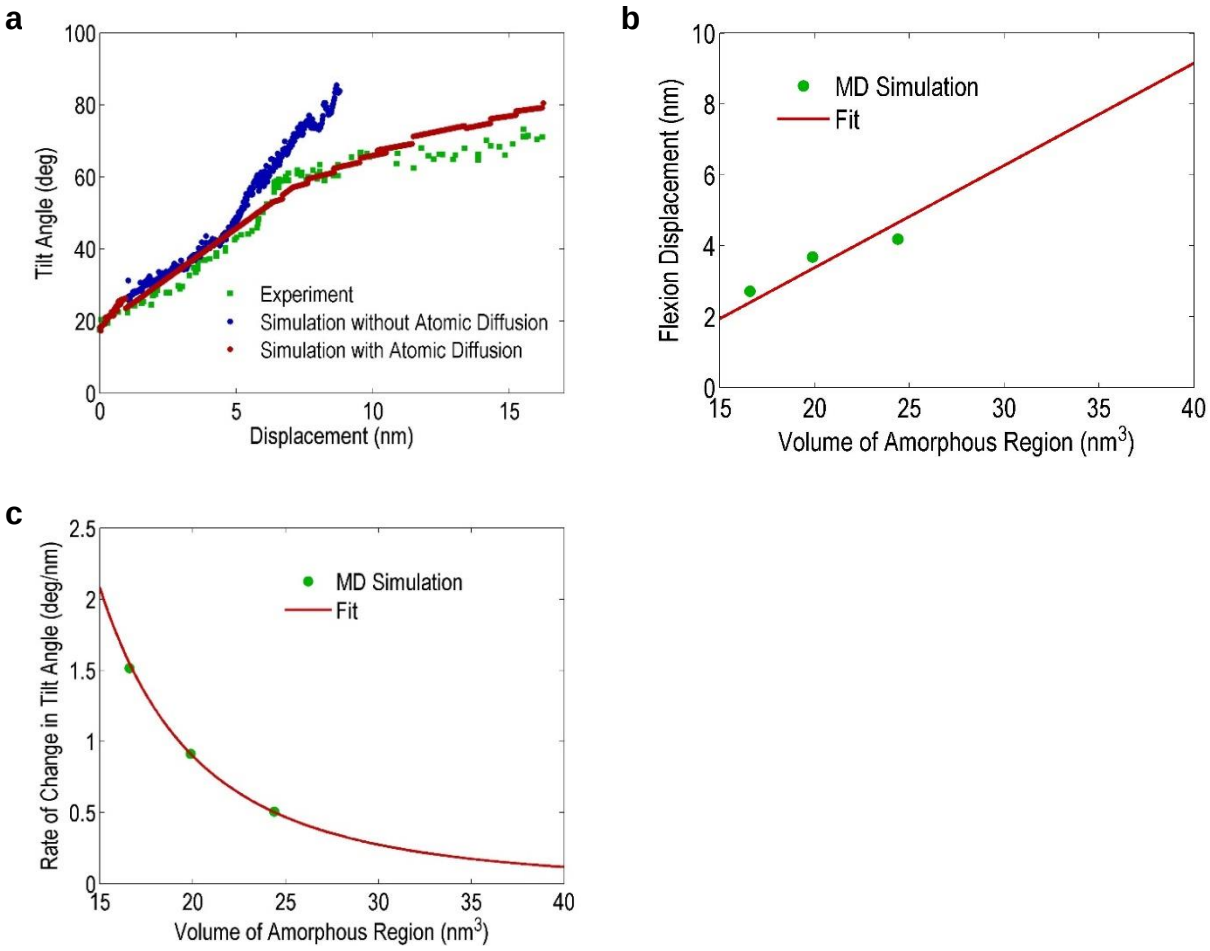

Figure S6. Influence of stress-assisted surface diffusion of atoms on the tilt angle of the anvil junction. (a) Tilt angle with and without stress-assisted surface diffusion of atoms. The continuous increase in the volume of the amorphous region accounts for the decreased rate of change in the tilt angle at displacements after about 6 nm. (b) Flexion displacement as a function of the volume of the amorphous region. As in Supporting Information Figure S5, in order to estimate the effect of stress-assisted surface diffusion on the tilt angle, we determined the relation between the volume of the amorphous region and the flexion displacement by fitting the MD simulation data with a linear function. Here the flexion displacement is defined to be the displacement at which the rate of change in tilt angle varies radically (i.e., about 5 nm in the actual observation). (c) Rate of change in tilt angle as a function of the volume of the amorphous

region at displacement values above the flexion displacement. We determined the rate of change in tilt angle as a function of the volume of the amorphous region by fitting the MD simulation data with an inverse cubic function. Finally, as in Supporting Information Figure S5, we segmented the total displacement by a factor of 17 for a constant increase rate of 5% and then patched the different sections of the functions together to obtain the function shown in (a).

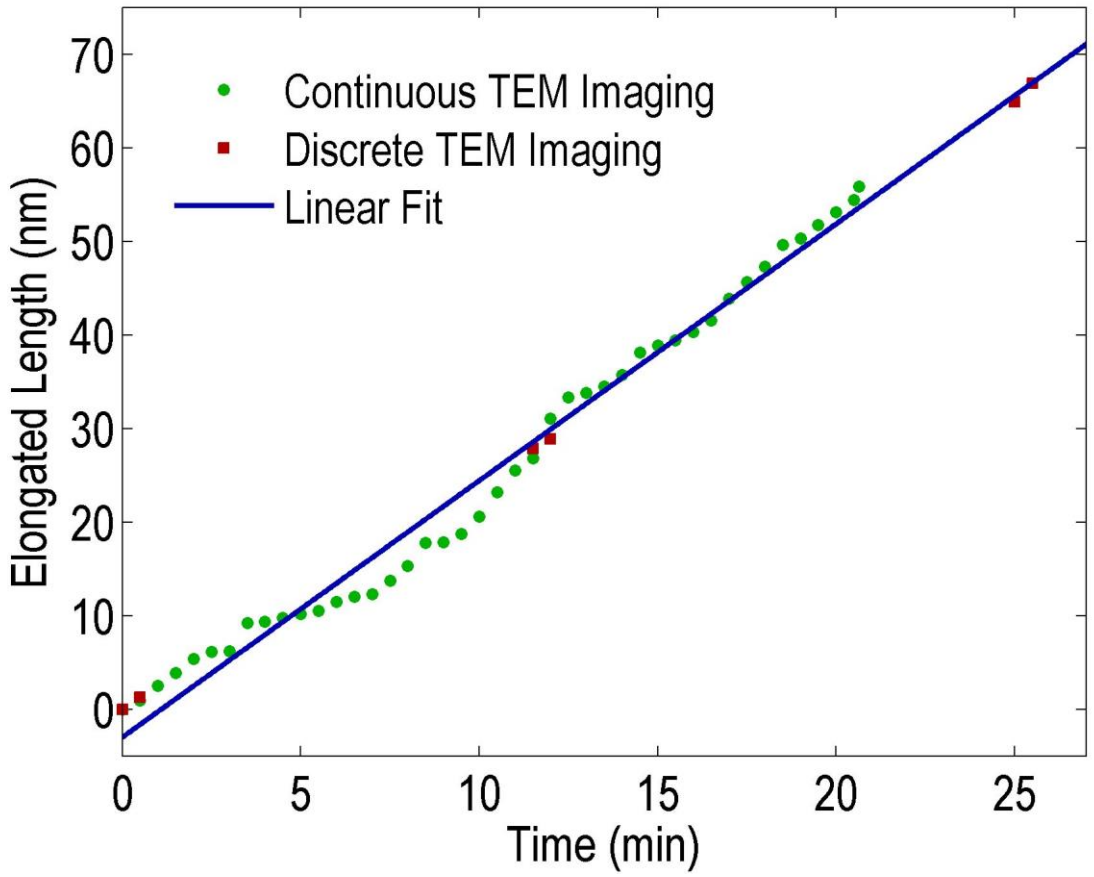

Figure S7. Potential influence of the electron beam in the TEM on the plastic deformation of the anvils. In order to verify that the influence of the electron beam in the TEM on the plastic deformation of the anvils is negligible, we performed continuous and discrete TEM measurements of the elongation of the anvil junction. Specifically, we compressed the upper

anvil onto the lower anvil and then pulled the upper anvil in the reverse direction while monitoring the evolution (i.e., elongation) of the anvil junction with the TEM. This figure indicates that there is no appreciable difference between the two measurements and hence, the effect of the electron beam on the plastic deformation is negligible. Here the maximum elongated lengths in the two measurements are different due to the difference in the initial junction diameter between them (junction diameter = 31.5 nm for the continuous TEM measurement and junction diameter = 39.0 nm for the discrete TEM measurement).

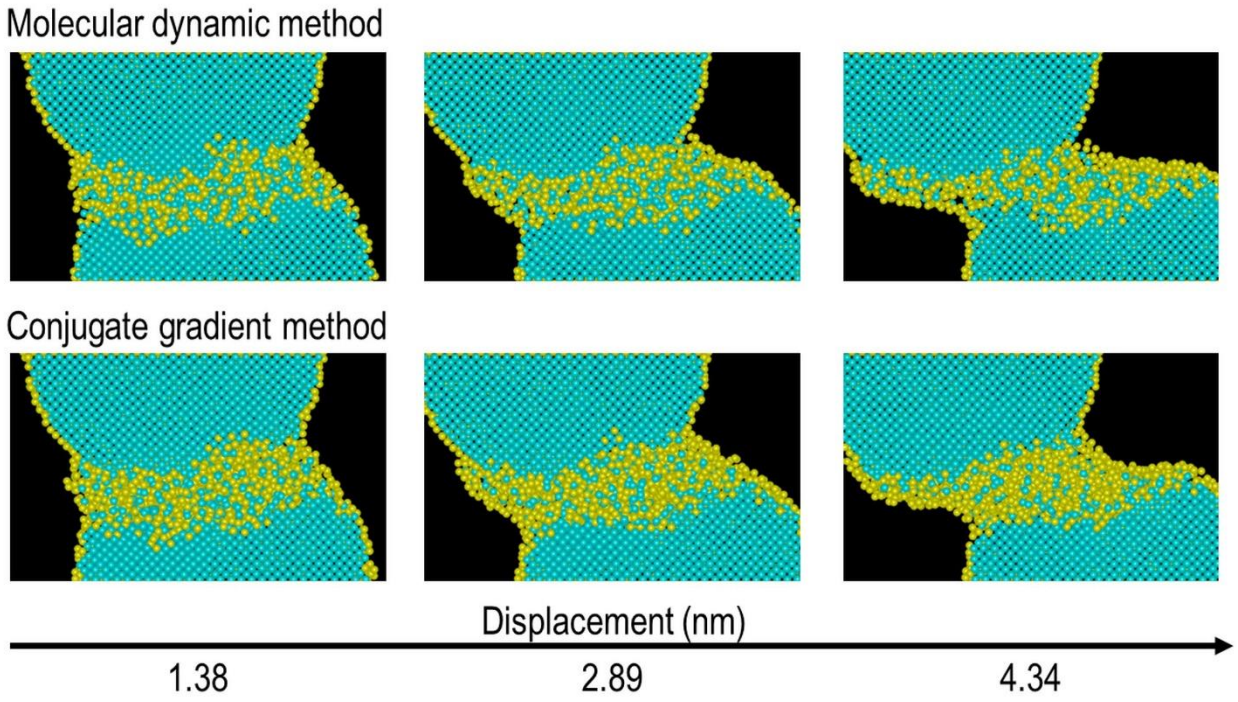

Figure S8. Comparison in junction deformation between molecular dynamics (MD) and conjugate gradient (CG) simulations. In order to verify that the MD method can simulate low-speed sliding as demonstrated in our time-lapse nanoscopy experiment, here we show the shear deformation of the junction using the CG method that simulates sliding dynamics at a quasi-static speed under a temperature of 0 K. The figure indicates that there is qualitatively no

significant difference in morphology between the MD and CG simulations. The average differences in junction diameter and tilt angle between the two methods are 0.09 nm and 2.08 degrees, respectively, meaning that they are quantitatively in good agreement as well.

	Normalization factor for displacement	Normalization factor for junction diameter	Initial tilt angle (deg)	Normalization factor for tilt angle
data0	16.201	5.500	17.586	53.561
data1	8.774	9.206	26.288	43.436
data2	14.92	11.762	19.558	49.795
data3	6.169	4.447	55.62	17.035
data4	74.791	31.13	-4.642	90.05
data5	4.516	3.675	15.255	52.451

Table S1. Normalization factors. The factors are used for the displacement, junction diameter, and tilt angle and the initial tilt angle to plot Supporting Information Figure S4 from the raw data.

Movie S1. Time-lapse movie of plastic deformation obtained with the TEM. At t = 0 min, the lower anvil starts to be displaced in the lateral direction at 0.01 nm/s and the anvils are induced to plastically deform. As the plastic deformation further progresses, the tilt angle continues to increase until the anvils finally break off at t = 19 min. The frame rate and duration of the movie are modified to 1.5 fps (30 fps in the original image acquisition) and 40 s (19 min in the original image acquisition), respectively.

Movie S2. MD simulation of plastic deformation. The lower anvil starts to be displaced in the lateral direction, inducing the anvil junction to plastically deform. As the plastic deformation further progresses, the tilt angle continues to increase until the anvils finally break off. Here the

cyan and yellow areas in the movie represent the crystalline and amorphous structures in which the total energy of each atom is smaller and larger than -4.1 eV, respectively.

Supporting References

(S1) Ishida, T.; Nakajima, Y.; Kakushima, K.; Mita, M.; Toshiyoshi, H.; Fujita, H. *J. Micromech. Microeng.* **2010**, 20, 075011.

(S2) Rudin, L.I.; Osher, S.; Fatemi, E. *Physica D* **1992**, 60, 259-268.

(S3) Chambolle, A. *J. Math. Imaging. Vis.* **2004**, 20, 89-97.

(S4) Caturla, M.J.; de la Rubia, T.D.; Gilmer, G.H. *J. Appl. Phys.* **1995**, 77, 3121-3125.